www.sciencemag.org/cgi/content/full/335/6074/1326/DC1

Supporting Online Material for

Laser Scribing of High-Performance and Flexible Graphene-Based Electrochemical Capacitors

Maher F. El-Kady, Veronica Strong, Sergey Dubin, Richard B. Kaner*

*To whom correspondence should be sent. E-mail: kaner@chem.ucla.edu

Published 16 March 2012, *Science* **335**, 1326 (2012)
DOI: 10.1126/science.1216744

This PDF file includes:

Other Supporting Online Material for this manuscript includes the following:
(available at www.sciencemag.org/cgi/content/full/335/6074/1326/DC1)

Movie S1

Materials and Methods

1. Synthesis of Laser Scribed Graphene (LSG) electrodes: GO was synthesized from high purity graphite powder using a modified Hummer's method as reported previously (33). Dispersions of GO in water (3.7 mg/mL) were then used to make GO films on various substrates, including polyethylene terephthalate (PET), nitrocellulose membrane (with 0.4 μm pore size), aluminum foil, and regular Xerox paper, among others. GO films were made by either drop-casting or vacuum filtering GO dispersions onto substrates that were previously cut to the size of a CD/DVD media disc. The films were then allowed to dry for 24 hours under ambient conditions (**Fig. S1**). These films were affixed on top of a LightScribe enabled DVD media disc and moved into the DVD optical drive for laser treatment. LightScribe is a direct labeling technology that patterns text and graphics onto the surface of a CD/DVD disc. LightScribe DVD drives are commercially available for ~ $20 and the LightScribing process is completely controlled by a standard desktop computer. The drive uses a laser (optimum power output = 5 mW, wavelength = 788 nm) to pattern a computer-generated image onto a light sensitive dye that changes color when hit with the laser; here, we use the GO film instead. The images are patterned in concentric circles, moving outward from the center of the disc as shown schematically in **Fig. 1**. The laser irradiation process results in the removal of oxygen species and the re-establishment of the sp^2 carbons. This causes a change in the conductivity of the film from the insulating graphite oxide, with a typical resistance of >20 MΩ/sq to highly conducting laser scribed graphene. We have shown that the number of times a film is laser-treated results in a significant and controllable change in conductivity (17). The electrodes used in the fabrication of the electrochemical capacitors are laser irradiated 6 times reaching an excellent conductivity of 1738 S/m. The laser irradiation process takes about 20 min per cycle. The produced laser scribed graphene (LSG) possesses very low oxygen content (only 3.5%) (17) that contributes to the very high cycling stability of the electrochemical capacitor. The thickness of the LSG layer, as measured from cross-sectional SEM and profilometry, was found to be ~7.6 μm (**Fig. S2**). In the actual device, the area made accessible to the electrolyte was 1 cm^2, which corresponds to a mass of 36.3 μg of the active material (LSG) per electrode or 72.8 μg for the device.

2. Electromechanical properties of laser scribed graphene electrodes: Flexible electronics have impacted our life in several ways, including flexible transistors, sensors, displays, etc. They are made possible by using flexible, mechanically robust and highly conducting electrodes. Nowadays, there is a great interest in using graphene films as flexible electrodes in these devices because of its excellent electrical, mechanical and optical properties (34). Here, we have investigated the electromechanical properties of the LSG electrodes to explore their potential for flexible devices. **Fig. S3A** shows the change in the resistance of an LSG electrode as a function of its bending radius. The electrical resistance shows a small decrease (2.8%) upon bending and this change is completely reversible by straightening the electrode back to its original flat state. Interestingly, the electrical resistance of the electrodes fluctuated up and down with only ~1% change after 1000 repeated bending cycles, **Fig. S3B**. Thus, LSG electrodes hold promise for other flexible electronics besides the electrochemical capacitors discussed in this paper.

3. Measurement of the specific surface area of laser scribed graphene: The surface area for the LSG was calculated to be ~1520 m^2/g using the methylene blue adsorption method. Methylene blue is a common dye probe used to determine the surface area of graphitic materials, with each molecule of adsorbed methylene blue representing 1.35 nm^2 of surface area (35-38). The surface area was calculated by adding a known mass of LSG into a standard concentration of methylene blue in DI water. LSG was stirred in the methylene blue solution continuously at a rate of 300 rpm for a total of 24 hr to reach maximum adsorption. The mixture was then allowed to settle and further centrifuged to remove any suspended material. The methylene blue concentration was determined by analyzing the supernatant through UV-vis spectroscopy at a wavelength of 665 nm and compared to the initial standard concentration of methylene blue prior to interacting with LSG.

4. Fabrication of LSG electrochemical capacitors: A simple device architecture has been employed to make the LSG electrochemical capacitors. Two LSG films serve as both electrodes and current collectors in a symmetric two-electrode cell configuration. LSG films made on various substrates are flexible and mechanically robust and thus can be directly used as electrochemical capacitor electrodes without any additional binders or conductive additives. Additionally, the high conductivity of the LSG films enables the construction of devices without the need for metallic current collector electrodes used in commercial electrochemical capacitors. In a typical device, an ion-porous separator [Celgard® 3501, (Celgard, Charlotte, NC)] was sandwiched between two identical pieces of LGC films (area, ~2 cm^2) in a layered structure (see **Fig. 1**). This layered assembly was wrapped with Kapton tape and then dipped in the electrolyte. To evaluate the electrochemical capacitor performance, the device was connected to an electrochemical workstation using alligator clips. Electrode edges were lightly painted with conducting silver paint to ensure good electrical contact between the LSG films and the alligator clips. The dimensions of the device and volume are shown in **Fig. S4**. Celgard® 3501 separators were generously supplied by Celgard, LLC Corporate Headquarters in Charlotte, NC, USA.

5. Fabrication of all-solid-state flexible LSG electrochemical capacitors: All solid-state devices were assembled by pouring the polymer gelled electrolyte (100 µL electrolyte/1 cm^2 of the electrode) slowly onto the LSG electrodes. This assembly was left under ambient conditions for 5 hours to ensure that the electrolyte completely wets the electrode and to allow for evaporation of any excess water. Two electrodes were then assembled face-to-face and left overnight until the electrolyte solidified. This results in mechanically robust devices with the polymer electrolyte acting as both the electrolyte and the ion-porous separator. The solidified polymer electrolyte simplifies the device architecture and helps maintain the electrodes in closer proximity.

5. Preparation of the polymer gelled electrolyte: The gelled electrolyte was prepared according to the method described in reference (39). Briefly, polyvinyl alcohol (PVA) (molecular weight 89,000-98,000, 99% hydrolyzed, Sigma-Aldrich) powder was mixed with water (1 g PVA/10 g H_2O). The mixture was heated at ~90 °C under constant stirring until the solution turned clear. After cooling under ambient conditions, 0.8 g of concentrated phosphoric acid solution (85% solution in water, Fisher Scientific) was added and the solution was stirred thoroughly.

6. Characterization of the electrochemical capacitors: The performance of our prototype electrochemical capacitors were evaluated by cyclic voltammetry (CV), galvanostatic charge/discharge (CC) curves using a VersaSTAT3 electrochemical workstation (Princeton Applied Research, USA). The electrochemical capacitor performances were evaluated in various electrolytes including aqueous and organic electrolytes as well as ionic liquids. Two different aqueous electrolytes were used, 1.0 M H_3PO_4 and 1.0 M H_2SO_4 (Sigma-Aldrich). The organic electrolyte consisted of 1.0 M tetraethylammonium tetrafluoroborate (Simga-Aldrich) in dry acetonitrile (Sigma-Aldrich). The ionic liquid, 1-ethyl-3-methylimidazolium tetrafluoroborate ($EMIMBF_4$) was obtained from Sigma-Aldrich and was used without further treatment. Electrochemical impedance spectroscopy (EIS) was carried out on a Solartron electrochemical workstation (Solartron Analytical, Oak Ridge, TN). EIS experiments were carried out at open circuit potential with a sinusoidal signal with amplitude of 10 mV over a frequency range of 100 kHz to 10 mHz. The sheet resistance and conductivity values were calculated from two-point probe measurements and the film thicknesses. The morphologies of GO and LSG were imaged using scanning electron microscopy (JEOL 6700, Philips XL 30). The film thicknesses of each layer in the device (e.g., the penetration depth of the laser into the GO layer, LSG layer, gelled polymer layer, etc.) were measured on a Dektak 6 profilometer and using cross-sectional scanning electron microscopy. The device dimensions are summarized in **Fig. S4**.

7. Characterization of commercial capacitors: A commercially available activated carbon electrochemical capacitor, PANASONIC EECS0HD223H Supercap 5.5 V, 22 mF was used. It consists of two electrochemical capacitors connected in series. A single device was separated from this serial assembly for characterization. An aluminum electrolytic capacitor, Mouser Electronics, 75-TE1066-E3, 3V/300μF was also tested. All the devices were characterized under the same dynamic conditions as the LSG-EC.

8. Tandem electrochemical capacitors: To be useful as energy storage devices in vehicles and peak-load applications, tandem electrochemical capacitors are usually assembled in series, in parallel or in combinations of the two. By choosing different tandem electrochemical capacitor assemblies, it is possible to control and improve the output potential and current (capacitance) so that the energy and power requirements can be met. Tandem LSG electrochemical capacitors were made simply by wiring four devices together in series, in parallel and in series-parallel combinations and characterized as shown in **Figs. S12-S14**.

9. Calculations: The capacitance of each device was calculated from the galvanostatic (CC) curves at different current densities using the formula:

$$C_{device} = i/(-dV/dt) \qquad (1)$$

Where i is the current applied (in amps, A), and dV/dt is the slope of the discharge curve (in volts per second, V/s). Specific capacitances were calculated based on the area or the volume of the device stack according to the following formulae:

$$\text{Areal capacitance} = C_{device}/A \qquad (2)$$

$$\text{Volumetric stack capacitance} = C_{device}/V \qquad (3)$$

Where A and V refer to the area (cm^2) and the volume (cm^3) of the device, respectively. It is worth mentioning that the volumetric capacitances were calculated taking into account the volume of the device stack. This includes the active material, the flexible substrate (or the current collector) and the separator with electrolyte. For the device testing, we did not include the packaging. The area and volume of the device used in the calculations can be found in **Fig. S4**.

The electrochemical performance of each device reported in **Fig. 5** is based on the volume of the stack and measured under the same dynamic conditions from galvanostatic curves. The power of each device was calculated from the galvanostatic curves at different charge/discharge current densities using the formula given in Equation (4):

$$P = (\Delta E)^2/4R_{ESR}V \qquad (4)$$

where P is the power (W/cm^3), ΔE is the operating voltage window (measured in volts and obtained from the discharge curve excluding the *IR* drop) and V is the volume of the stack as indicated earlier (in cm^3). R_{ESR} is the internal resistance of the device which can be estimated from the voltage drop at the beginning of the discharge, V_{drop}, at a constant current density (i) using the formula $R_{ESR} = V_{drop}/2i$.

The energy density of the device was obtained from the formula given in Equation (5):

$$E = C_V \times (\Delta E)^2/(2 \times 3600) \qquad (5)$$

where E is the energy density in Wh/cm^3, C_V is the volumetric stack capacitance obtained from Equation (3) in F/cm^3 and ΔE is the operating voltage window in volts.

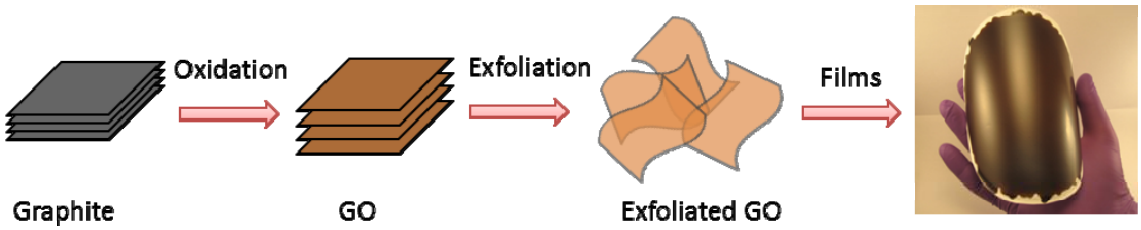

Fig. S1. Schematic illustration of the preparation of GO films: (A) The GO precursor is made by oxidation of graphite using a modified Hummer's method and then dispersed in water by ultrasonication. GO films are coated onto various flexible substrates such as polyethylene terephthalate, aluminum foil, a porous nitrocellulose membrane (shown in the photograph) or regular photocopy paper.

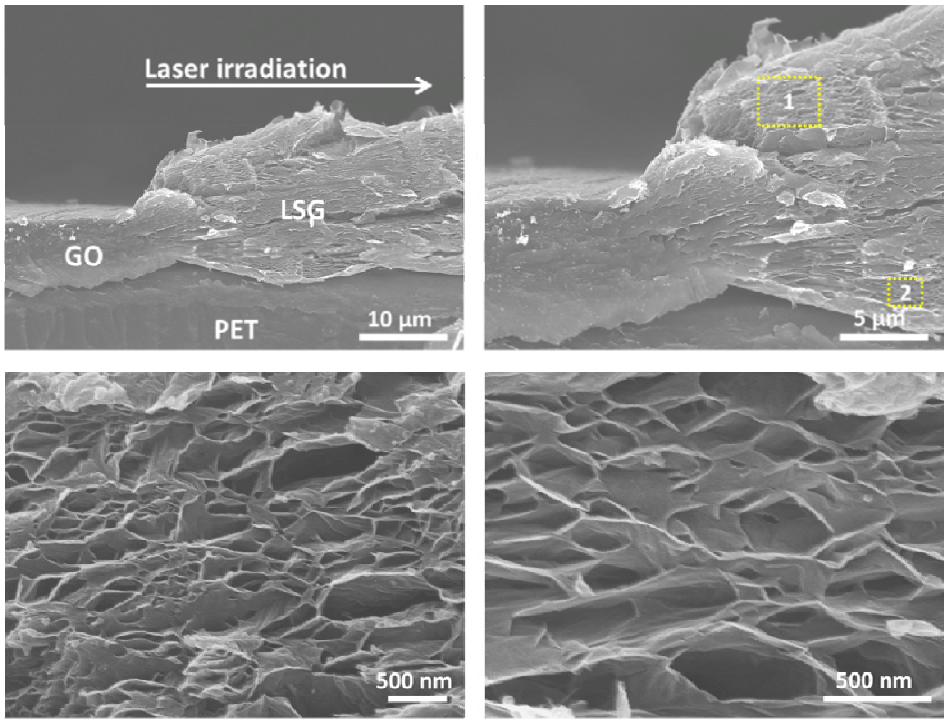

Fig. S2: Laser scribing of graphene from graphite oxide film on a polyethylene terephthalate (PET) flexible support. (A) A cross-sectional SEM image of the film at the interface between GO and LSG. As the LightScribe laser converts GO into LSG, a substantial expansion of the film is observed. (B) A zoomed-in view of the interface region. (C) and (D) show expanded views of the locations 1 and 2, respectively. The laser penetrates all the way into the film producing the expanded LSG network. The LSG electrode possesses a significant thickness and shows potential for electrochemical capacitors with high power and energy densities.

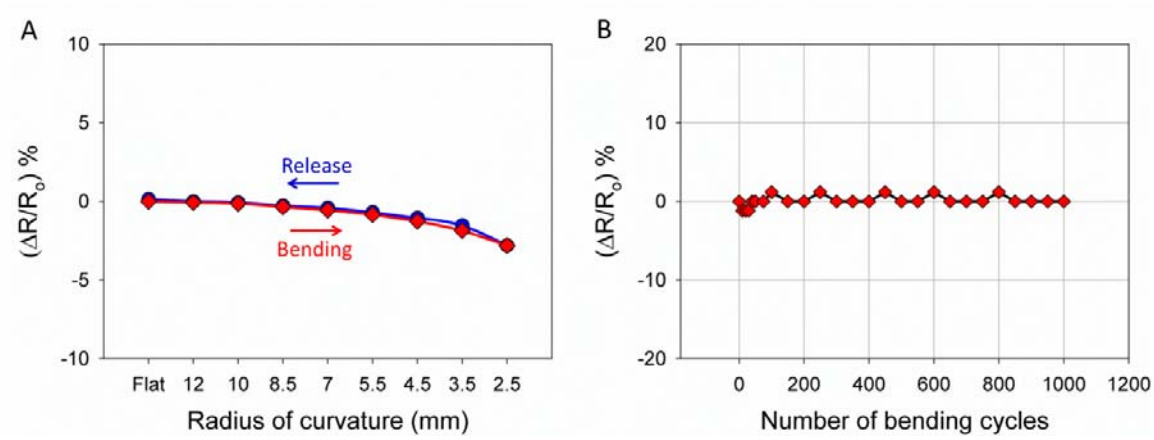

Fig. S3. Electromechanical properties of LSG electrodes made on polyethylene terephthalate (PET) flexible supports. (A) The electrical resistance change of an LSG electrode as a function of the bending radius. The electrode shows a decrease in the electrical resistance of ~2.8% and this change is completely reversible by flattening back the electrode to its original flat state. (B) The resistance change of an LSG electrode under repeated bending cycles for a bend radius of 5 mm. Only a slight change in resistance of ~1% can be observed after 1000 repeated bending cycles.

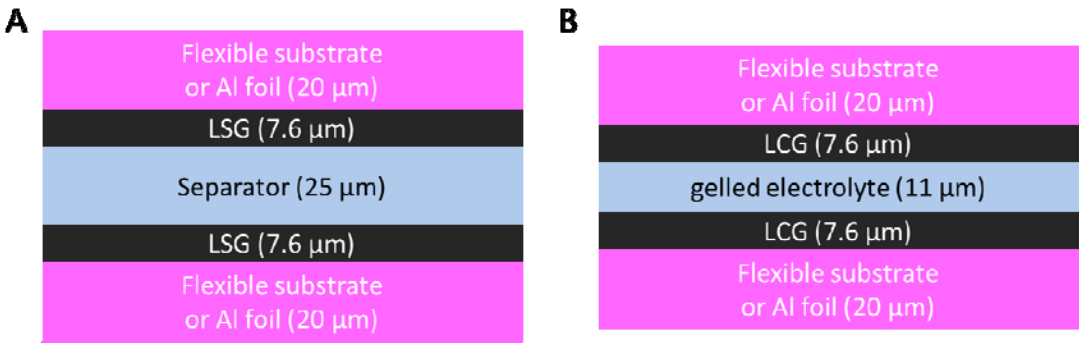

Fig. S4: Schematic diagrams showing cross-sections of the electrochemical capacitors with their device dimensions. (A) Two LSG electrodes are supported on a flexible substrate or an Al foil current collector and separated with an organic ion-porous separator [Celgard® 3501 (Celgard, Charlotte, NC)]. The electrolyte wets the LSG layer and the separator. This design of the electrochemical capacitor was tested in a variety of electrolytes including aqueous, organic and ionic liquid electrolytes. The device effective thickness is 82.2 µm, with an active area of 1 cm^2 and a volume of 8.22×10^{-3} cm^3. (B) In an all solid-state device, the organic separator is replaced with a gelled electrolyte that has a thickness of 11 µm and thus the device thickness becomes 68.2 µm with a volume of 6.82×10^{-3} cm^3.

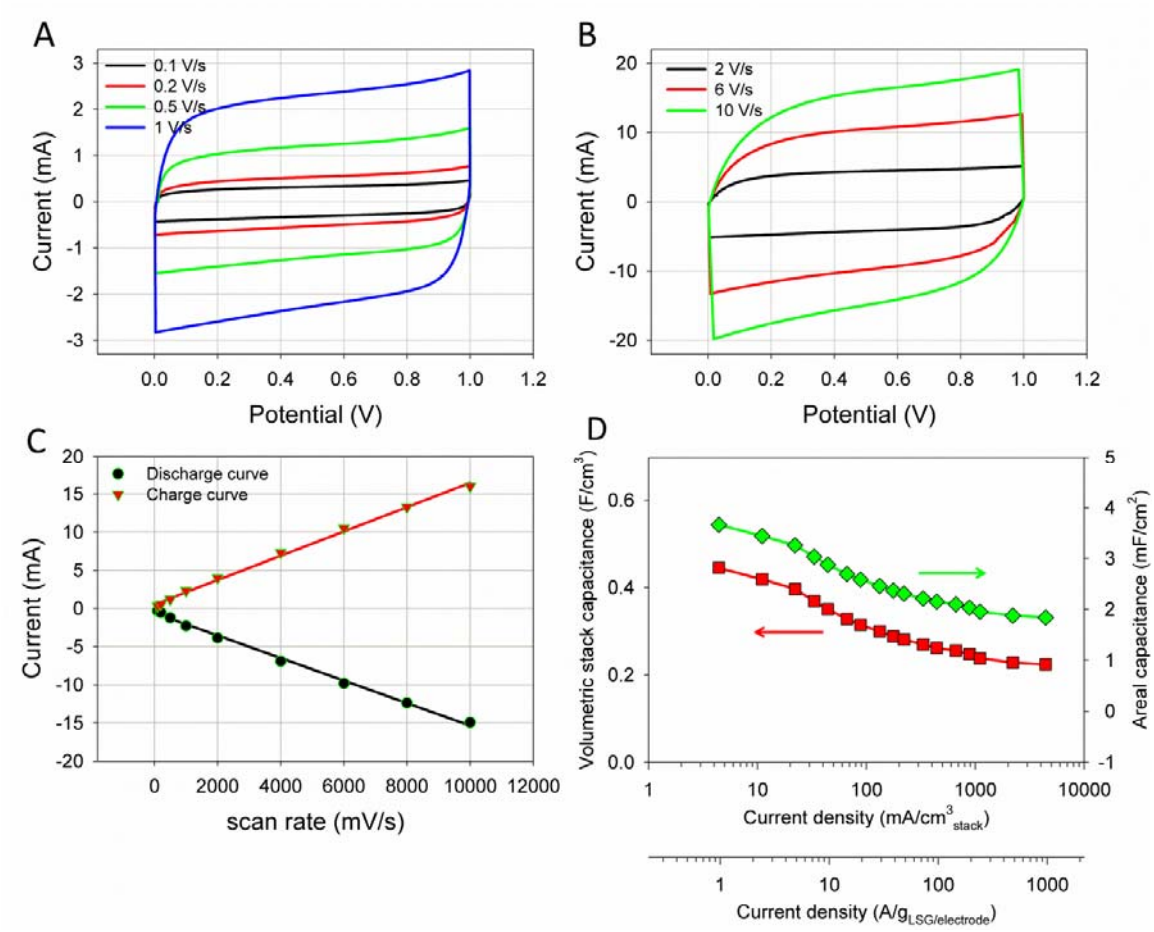

Fig. S5: Performance of an LSG electrochemical capacitor over a wide range of scan rates: cyclic voltammetry profiles of an LSG electrochemical capacitor in aqueous 1.0 M H_3PO_4 at different scan rates: (A) 100 mV/s to 1000 mV/s; and (B) 2000 mV/s to 10,000 mV/s. (C) The dependence of the capacitive current (extracted from the CV profiles at 0.5 V for the charge and discharge curves) on the applied scan rate. A linear relationship is observed with $R^2 = 0.997$ and 0.996 for the charge and discharge curves, respectively. (D) The specific capacitance of the device calculated from the galvanostatic curves as a function of the charge/discharge current density. The specific capacitance data are presented on the basis of the area of the device or the volume of the entire device stack (**Fig. S4**). Note that the current density shown is based on the volume of the whole stack or the mass of the LSG in one electrode. The areal capacitance of the LSG-EC was calculated to be 3.67 mF/cm^2 at 1 A/$g_{LSG/electrode}$. This translates to a gravimetric capacitance of 202 F/$g_{LSG/electrode}$.

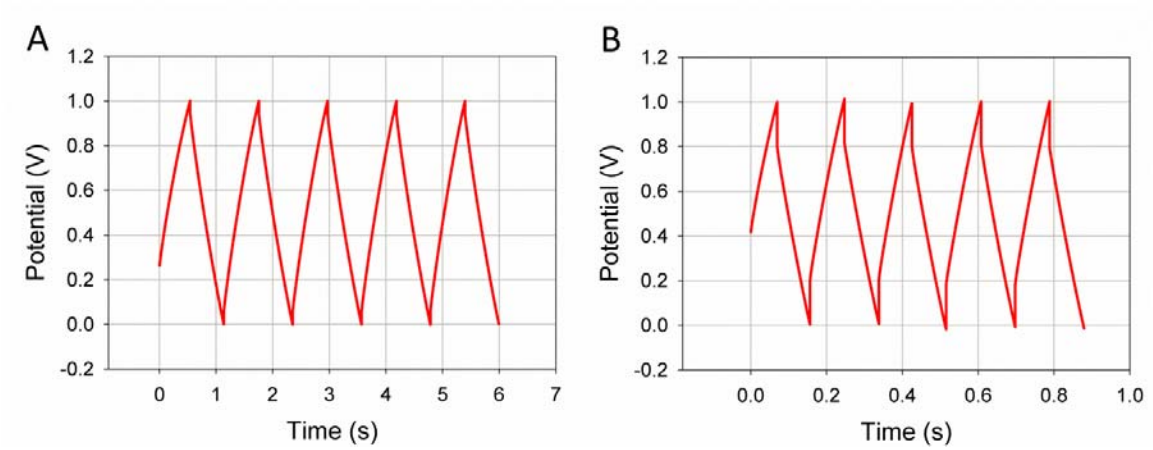

Fig. S6: Capability of an LSG electrochemical capacitor for ultrafast charging and discharging in the sub-second time scale as tested in aqueous 1.0 M H_3PO_4: galvanostatic charge/discharge curves obtained at ultrahigh current densities of (A) 100 A/g; and (B) 500 A/g (based on the mass of the LSG per electrode). As can be seen in B, the device can be efficiently charged/discharged multiple times in less than a second.

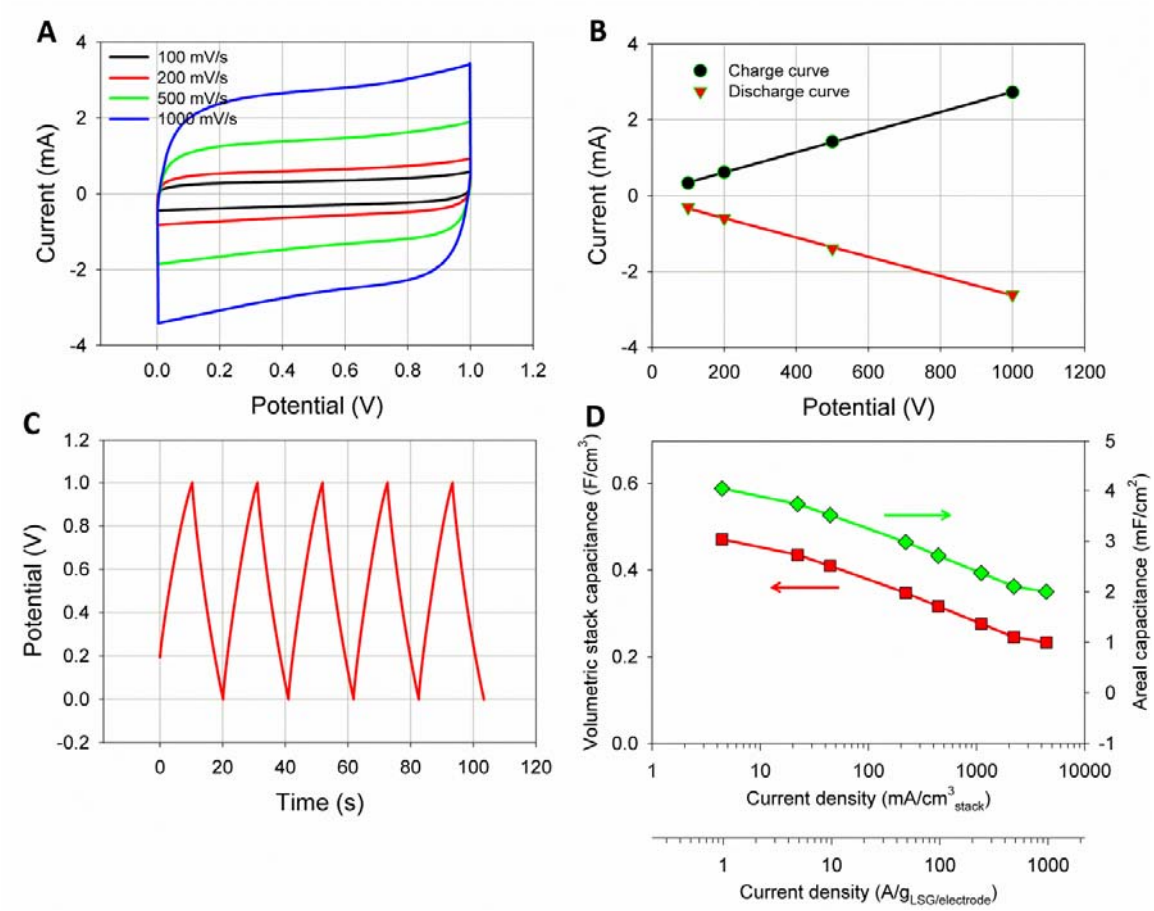

Fig. S7: Performance of an LSG electrochemical capacitor in aqueous 1.0 M H_2SO_4: (A) Nearly rectangular CV profiles are observed at increasing potential scan rates from 100 to 1000 mV/s. (B) A linear relationship is obtained between the capacitive current (extracted from the CV profiles at 0.5 V for the charge and discharge segments) and the scan rate with $R^2 = 0.9998$ for both curves. This trend confirms the formation of a pure electrostatic double layer. (C) Galvanostatic curves obtained at 10 $A/g_{LSG/electrode}$; the device exhibits a voltage drop of only 0.014 V at the beginning of the discharge curve. This corresponds with a low internal resistance for the device. (D) Specific capacitance (areal and volumetric) as a function of the charge/discharge current density. The device shows an areal capacitance of 4.04 mF/cm^2 at 1 $A/g_{LSG/electrode}$ which translates to a gravimetric capacitance of 222 $F/g_{LSG/electrode}$.

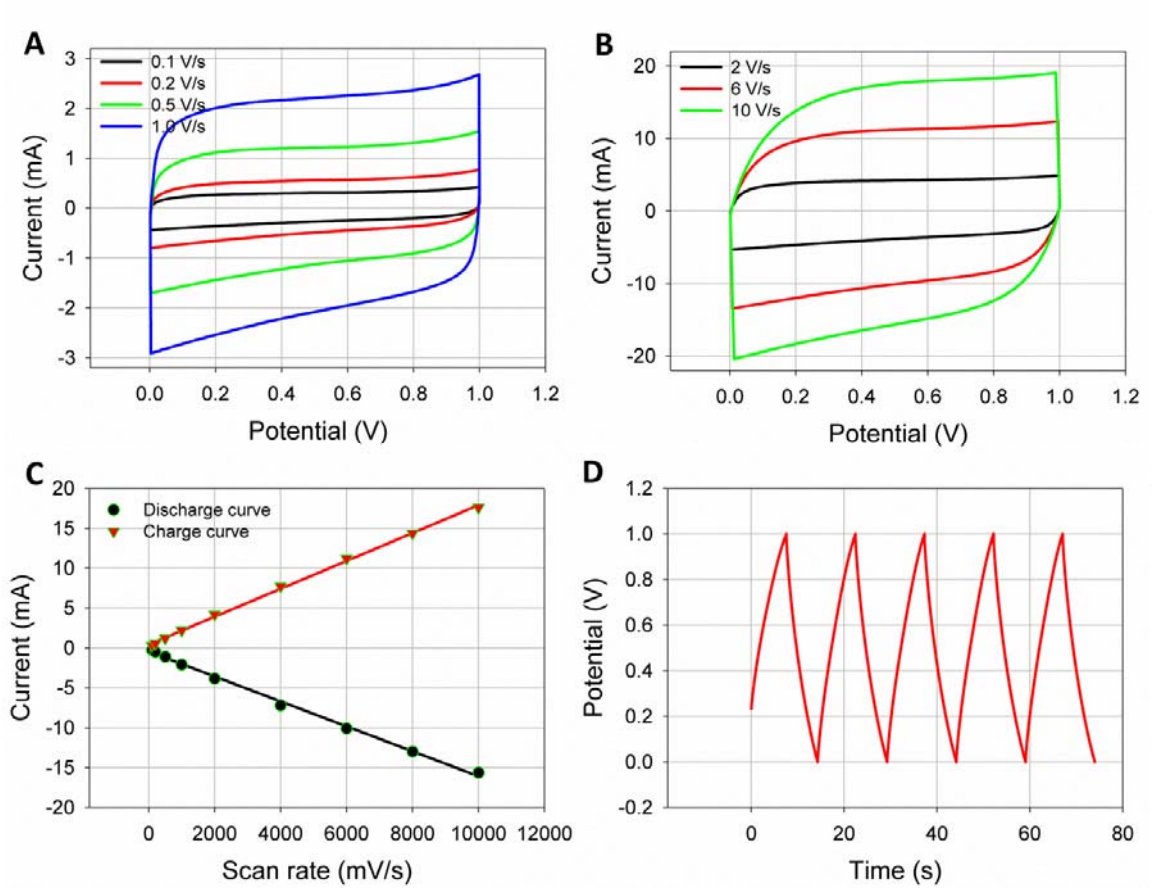

Fig. S8: Performance of an LSG electrochemical capacitor when supported on a nitrocellulose membrane in aqueous 1.0 M H_3PO_4: (A) CV profiles at different scan rates (A) from 100 to 1000 mV/s and (B) from 2,000 to 10,000 mV/s. Nearly rectangular CV profiles are obtained at all the scan rates; (C) A linear relationship is observed between the capacitive current (extracted from the CV profiles at 0.5 V for the charge and discharge segments) and the scan rate with R^2 = 0.9985 and 0.9970 for the charge and discharge curves, respectively. (D) Galvanostatic curves obtained at 10 $A/g_{LSG/electrode}$; the device exhibits a voltage drop of only 0.019 V at the beginning of the discharge curve. This corresponds to a very low internal resistance for the device. These data show that an LSG can be made on different substrates and still maintain its high performance.

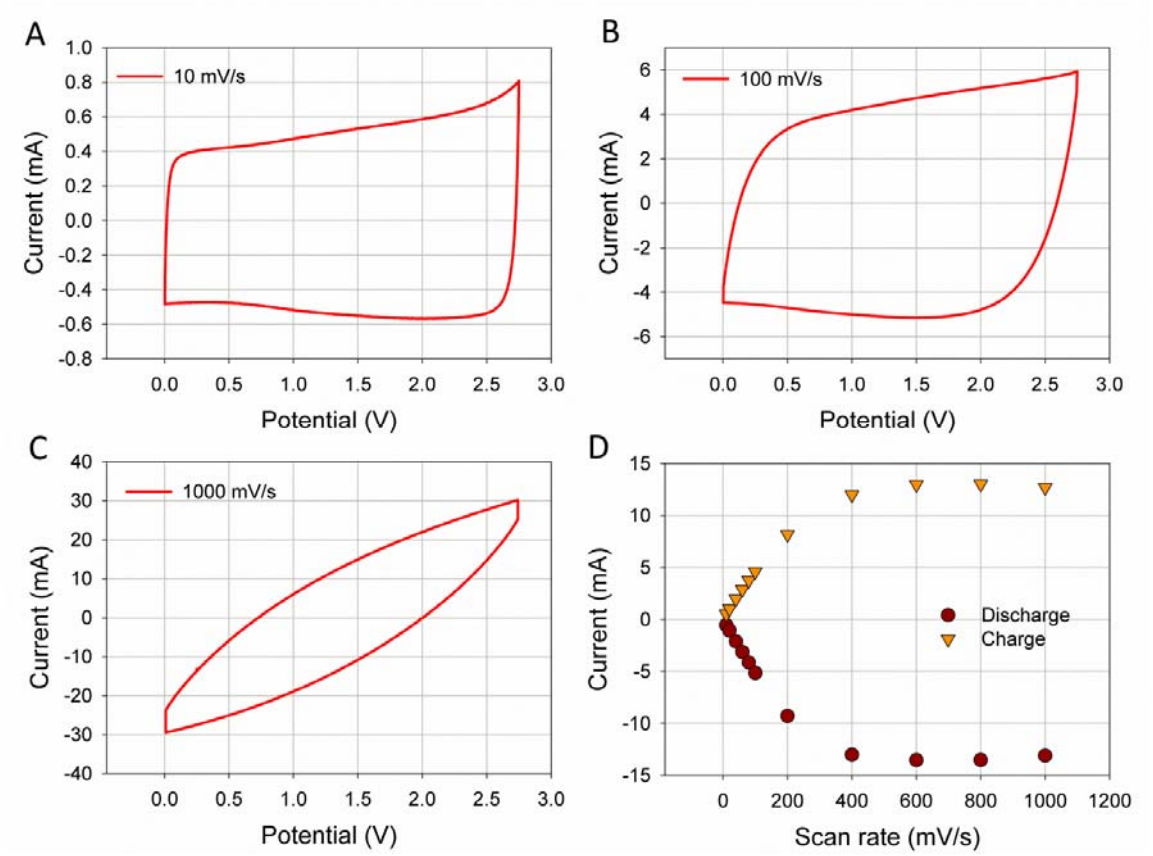

Fig. S9: Electrochemical characterization of the performance of a commercially available activated carbon electrochemical capacitor: CV profiles of the device shown in a potential window of 2.75 V at different scan rates of (A) 10 mV/s (B) 100 mV/s and (C) 1000 mV/s. In contrast to the LSG electrochemical capacitors, this commercial device exhibits the desired rectangular CV shape only at slow scan rates, 10 to 100 mV/s; (D) Dependence of the capacitive current (extracted from the CV profiles at 1.375 V) on the potential scan rate. A linear relationship is observed only between 10-100 mV/s, indicating the limited rate performance of this activated carbon electrochemical capacitor.

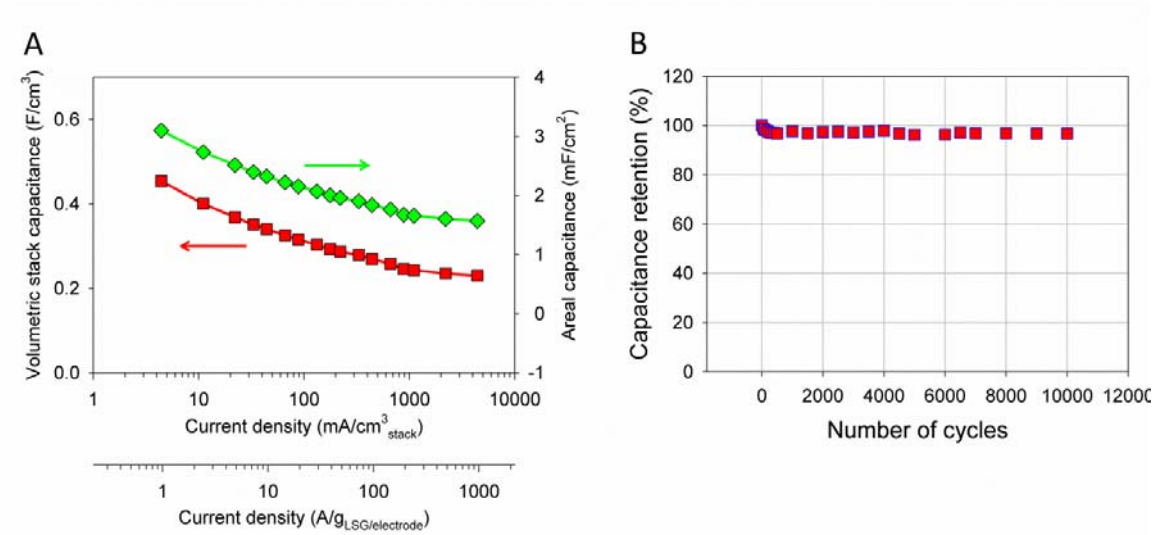

Fig. S10: Characterization of an all-solid state LSG electrochemical capacitor: (A) Areal and volumetric capacitance of the device as a function of the current density. (B) Cycling stability of an all solid-state LSG electrochemical capacitor: the device loses only about 3% of its capacitance after 10,000 cycles indicating very good cycling stability.

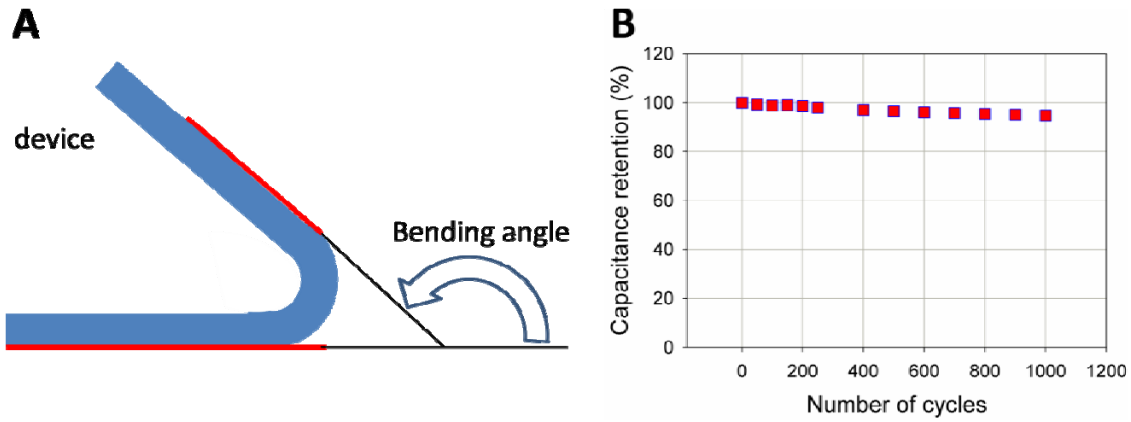

Fig. S11: Capability of an all solid-state LSG electrochemical capacitor for charge/discharge under bending conditions. (A) A schematic diagram showing the device under stress and defining the bend angle. (B) The device can be bent arbitrarily without any obvious decrease in performance compared to its planar state. The device retains about 95% of the initial capacitance after 1000 cycles when tested under the bent state (applying a bend angle = 150°).

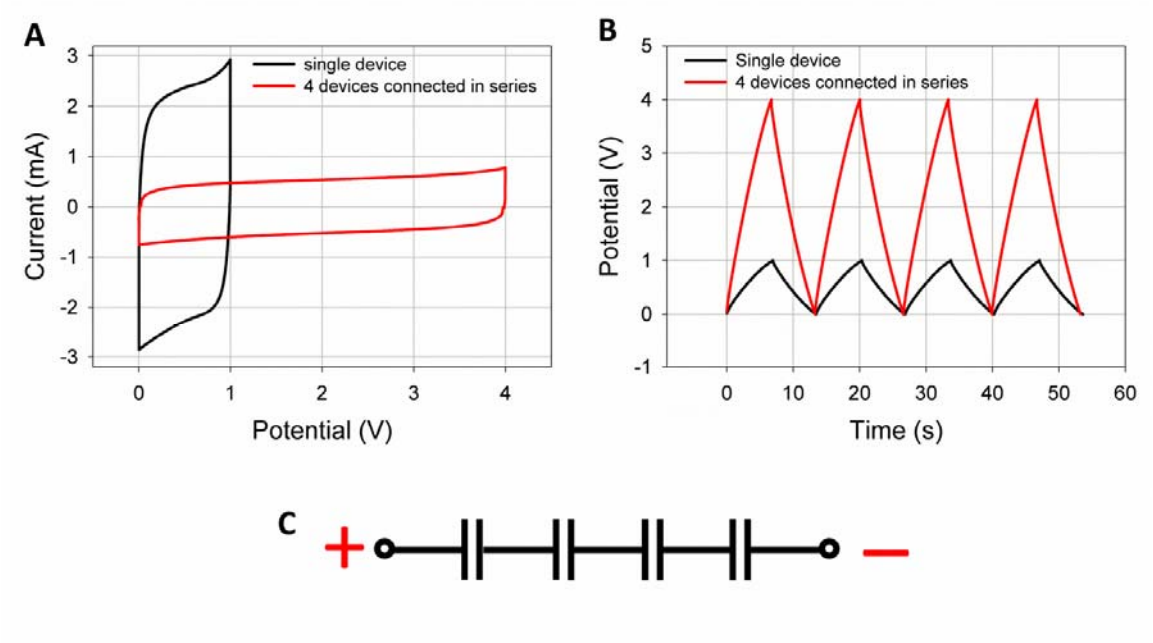

Fig. S12: Increasing the output voltage via tandem serial electrochemical capacitors: portable equipment needing higher voltages use device packs with two or more devices connected in series. Adding electrochemical capacitors together in a serial string increases the voltage, while the current remains the same. Here, the performance of an all solid-state electrochemical capacitor pack with 4 devices connected in series was tested. (A) Cyclic voltammetry at 1000 mV/s shows that the voltage is extended to 4 volts (vs. 1 volt for a single device), while the produced current (represented by the area under the curve) is essentially the same for the single device and for the cell pack; (B) Galvanostatic charge/discharge curves for a single device and for the cell pack were all operated under the same constant current conditions. As can be seen, at the same charge/discharge current, the voltage is extended from 1 volt for a single device to 4 volts for a cell pack. Interestingly, a very low voltage drop is observed in the CC curves of the device pack indicating low internal resistance. This helps optimize the useful energy that can be drawn from the device.

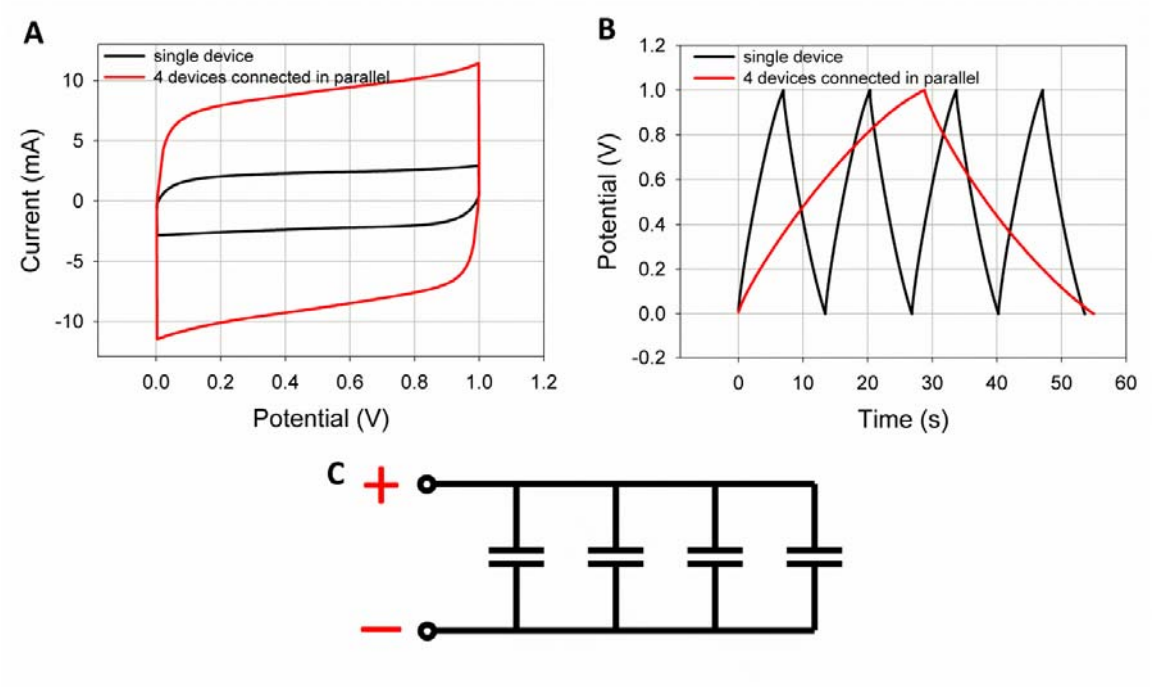

Fig. S13: Increasing the output current via tandem parallel electrochemical capacitors: If higher operating currents are needed, two or more cells can be connected in parallel. Putting electrochemical capacitors together in parallel enhances the output current, while the operating voltage remains the same. Here, the performance of an all solid-state electrochemical capacitor pack with 4 devices connected in parallel was tested; (A) Cyclic voltammetry at 1000 mV/s shows that the capacitive current increases by a factor of 4; (B) Galvanostatic charge/discharge curves for the single device and for the cell pack were all operated under the same constant current conditions. Clearly, the runtime of the electrochemical capacitor pack (and thus the ampere-hour rating) increases by a factor of 4 under the same charge/discharge current.

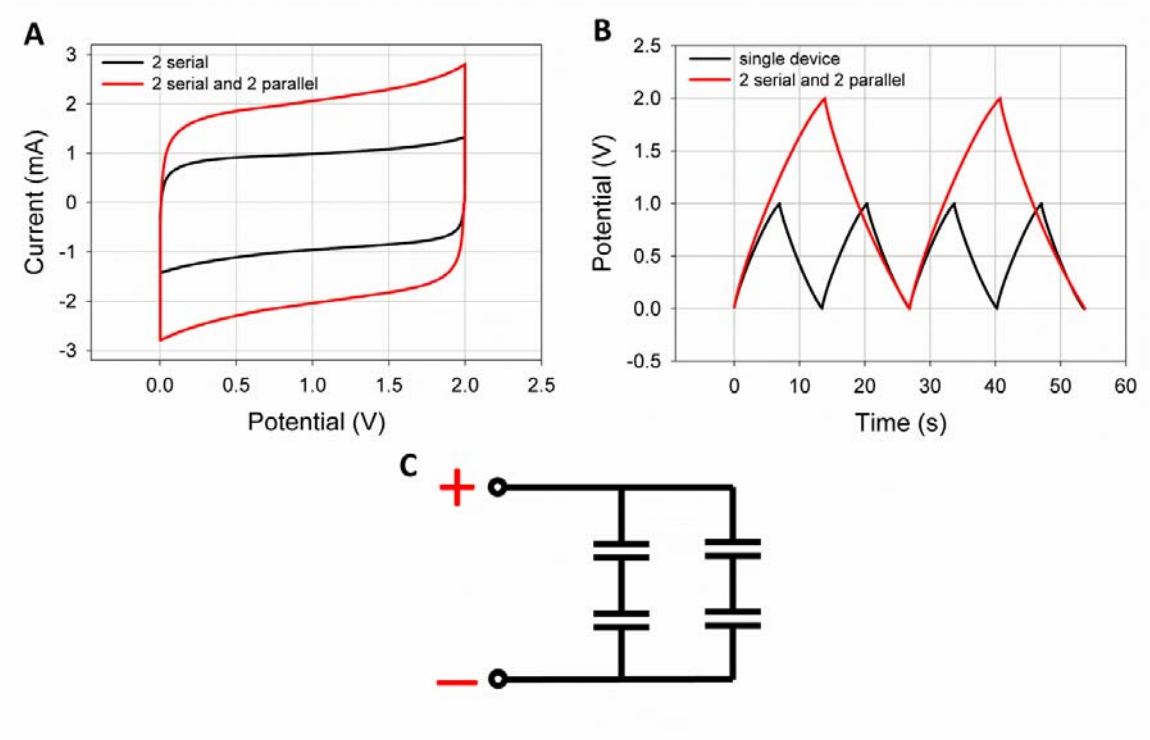

Fig. S14: Increasing the output voltage and current via tandem serial/parallel electrochemical capacitors: In a serial/parallel design, the electrochemical capacitors are connected in a way that produces both the required voltage and current. Here, the performance of an all solid-state electrochemical capacitor pack with 4 devices connected in serial/parallel as shown in C was tested: (A) Cyclic voltammetry at 1000 mV/s shows that both the output voltage and current increase by a factor of 2; (B) Galvanostatic charge/discharge curves for a single device and for the cell pack were all operated under the same constant current conditions. Clearly, both the output voltage and the runtime of the electrochemical capacitor pack increases by a factor of two under the same charge/discharge current.

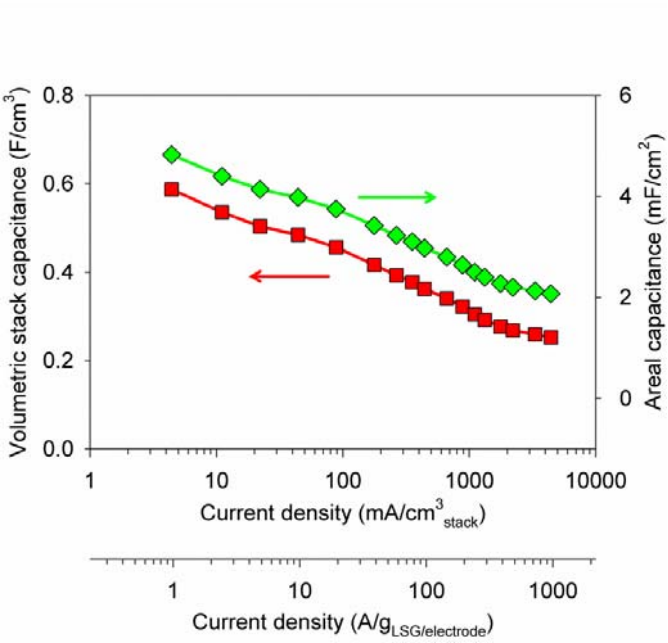

Fig. S15: The performance of an LSG electrochemical capacitor in an organic electrolyte of 1.0 M tetraethylammonium tetrafluoroborate (TEA-BF_4) in acetonitrile: The capacitance was calculated from the galvanostatic curves and represented in terms of the area or the volume of the device stack.

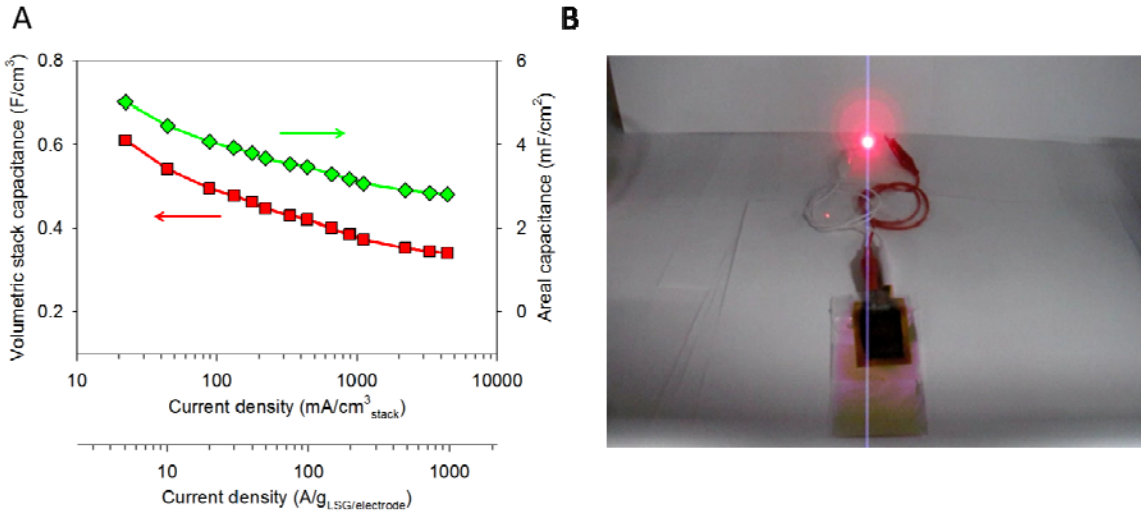

Fig. S16: Performance of an LSG electrochemical capacitor in the ionic liquid 1-ethyl-3-methylimidazolium tetrafluoroborate (EMIMBF$_4$). (A) Specific capacitance as calculated from the galvanostatic curves at different charge/discharge current densities. The electrochemical capacitor exhibits a high rate performance with a specific capacitance as high as ~5 mF/cm^2 (276 F/g based on the weight of the LSG on one electrode). (B) This charged electrochemical capacitor is used to light up a red light emitting diode.

Movie S1

In this movie an LSG electrochemical capacitor is packaged in the ionic liquid 1-ethyl-3-methylimidazolium tetrafluoroborate ($EMIMBF_4$). After charging the electrochemical capacitor at a constant potential of 3.5 V, it is used to light up a red light emitting diode (with a minimum operating potential of 2 V) for about 24 minutes.

References and Notes

1. C. Liu, F. Li, L.-P. Ma, H.-M. Cheng, Advanced materials for energy storage. *Adv. Energy Mater.* **22**, E28 (2010). doi:10.1002/adma.200903328

2. D. S. Su, R. Schlögl, Nanostructured carbon and carbon nanocomposites for electrochemical energy storage applications. *ChemSusChem* **3**, 136 (2010). doi:10.1002/cssc.200900182 Medline

3. P. Simon, Y. Gogotsi, Materials for electrochemical capacitors. *Nat. Mater.* **7**, 845 (2008). doi:10.1038/nmat2297 Medline

4. J. R. Miller, P. Simon, Materials science. Electrochemical capacitors for energy management. *Science* **321**, 651 (2008). doi:10.1126/science.1158736 Medline

5. D. Pech *et al*., Ultrahigh-power micrometre-sized supercapacitors based on onion-like carbon. *Nat. Nanotechnol.* **5**, 651 (2010). doi:10.1038/nnano.2010.162 Medline

6. J. Chmiola, C. Largeot, P. L. Taberna, P. Simon, Y. Gogotsi, Monolithic carbide-derived carbon films for micro-supercapacitors. *Science* **328**, 480 (2010). doi:10.1126/science.1184126 Medline

7. J. Xia, F. Chen, J. Li, N. Tao, Measurement of the quantum capacitance of graphene. *Nat. Nanotechnol.* **4**, 505 (2009). doi:10.1038/nnano.2009.177 Medline

8. M. Segal, Selling graphene by the ton. *Nat. Nanotechnol.* **4**, 612 (2009). doi:10.1038/nnano.2009.279 Medline

9. M. D. Stoller, S. Park, Y. Zhu, J. An, R. S. Ruoff, Graphene-based ultracapacitors. *Nano Lett.* **8**, 3498 (2008). doi:10.1021/nl802558y Medline

10. Y. Wang *et al*., Supercapacitor devices based on graphene materials. *J. Phys. Chem. C* **113**, 13103 (2009). doi:10.1021/jp902214f

11. Z. Weng *et al*., Graphene-cellulose paper flexible supercapacitors. *Adv. Energy Mater.* **1**, 917 (2011). doi:10.1002/aenm.201100312

12. Y. Zhu *et al*., Exfoliation of graphite oxide in propylene carbonate and thermal reduction of the resulting graphene oxide platelets. *ACS Nano* **4**, 1227 (2010). doi:10.1021/nn901689k Medline

13. W. Gao *et al*., Direct laser writing of micro-supercapacitors on hydrated graphite oxide films. *Nat. Nanotechnol.* **6**, 496 (2011). doi:10.1038/nnano.2011.110 Medline

14. C. G. Liu, Z. Yu, D. Neff, A. Zhamu, B. Z. Jang, Graphene-based supercapacitor with an ultrahigh energy density. *Nano Lett.* **10**, 4863 (2010). doi:10.1021/nl102661q

15. Y. Zhu *et al*., Carbon-based supercapacitors produced by activation of graphene. *Science* **332**, 1537 (2011). doi:10.1126/science.1200770 Medline

16. X. Yang, J. Zhu, L. Qiu, D. Li, Bioinspired effective prevention of restacking in multilayered graphene films: Towards the next generation of high-performance supercapacitors. *Adv. Mater. (Deerfield Beach Fla.)* **23**, 2833 (2011). doi:10.1002/adma.201100261

17. V. Strong *et al*., Patterning and electronic tuning of laser scribed graphene for flexible all-carbon devices. *ACS Nano* 120215095449007 (2012). doi:10.1021/nn204200w Medline

18. R. Chandrasekaran, Y. Soneda, J. Yamashita, M. Kodama, H. Hatori, Preparation and electrochemical performance of activated carbon thin films with polyethylene oxide-salt addition for electrochemical capacitor applications. *J. Solid State Electrochem.* **12**, 1349 (2008). doi:10.1007/s10008-008-0559-6

19. S. W. Lee, B. M. Gallant, H. R. Byon, P. T. Hammond, Y. Shao-Horn, Energy. *Energy Environ. Sci.* **4**, 1972 (2011).

20. H. Zhang, X. Yu, P. V. Braun, Three-dimensional bicontinuous ultrafast-charge and -discharge bulk battery electrodes. *Nat. Nanotechnol.* **6**, 277 (2011). doi:10.1038/nnano.2011.38 Medline

21. L. L. Zhang, X. S. Zhao, Carbon-based materials as supercapacitor electrodes. *Chem. Soc. Rev.* **38**, 2520 (2009). doi:10.1039/b813846j Medline

22. P. L. Taberna, P. Simon, J. F. Fauvarque, Electrochemical characteristics and impedance spectroscopy studies of carbon-carbon supercapacitors. *J. Electrochem. Soc.* **150**, A292 (2003). doi:10.1149/1.1543948

23. Y. Shim, Y. J. Jung, H. J. Kim, Graphene-Based Supercapacitors: A computer simulation study. *J. Phys. Chem. C* **115** 23574 (2011). doi:10.1021/jp203458b

24. X. Zhao *et al*., Carbon nanosheets as the electrode material in supercapacitors. *J. Power Sources* **194**, 1208 (2009). doi:10.1016/j.jpowsour.2009.06.004

25. J. R. Miller, R. A. Outlaw, B. C. Holloway, Graphene double-layer capacitor with ac line-filtering performance. *Science* **329**, 1637 (2010). doi:10.1126/science.1194372 Medline

26. J. R. Miller, R. A. Outlaw, B. C. Holloway, Graphene electric double layer capacitor with ultra-high-power performance. *Electrochim. Acta* **56**, 10443 (2011). doi:10.1016/j.electacta.2011.05.122

27. C. Du, N. Pan, Supercapacitors using carbon nanotubes films by electrophoretic deposition. *J. Power Sources* **160**, 1487 (2006). doi:10.1016/j.jpowsour.2006.02.092

28. C. Du, N. Pan, High power density supercapacitor electrodes of carbon nanotube films by electrophoretic deposition. *Nanotechnology* **17**, 5314 (2006). doi:10.1088/0957-4484/17/21/005

29. H. Nishide, K. Oyaizu, Toward flexible batteries. *Science* **319**, 737 (2008). doi:10.1126/science.1151831 Medline

30. D. W. Wang, F. Li, M. Liu, G. Q. Lu, H.-M. Cheng, 3D Aperiodic hierarchical porous graphitic carbon material for high-rate electrochemical capacitive energy storage. *Angew. Chem. Int. Ed.* **47**, 373 (2008). doi:10.1002/anie.200702721

31. D. Andrea, *Battery Management Systems for Large Lithium Ion Battery Packs* (Artech House, Norwood, MA, 2010).

32. J. F. Wishart, *Energy Environ. Sci.* **2**, 956 (2009).

33. N. I. Kovtyukhova *et al*., Layer-by-layer assembly of ultrathin composite films from micron-sized graphite oxide sheets and polycations. *Chem. Mater.* **11**, 771 (1999). doi:10.1021/cm981085u

34. Y. Zhu, Z. Sun, Z. Yan, Z. Jin, J. M. Tour, Rational design of hybrid graphene films for high-performance transparent electrodes. *ACS Nano* **5**, 6472 (2011) and references therein. doi:10.1021/nn201696g Medline

35. P. T. Hang, G. W. Brindley, Methylene blue absorption by clay minerals. Determination of surface areas and cation exchange capacities (Clay-Organic Studies XVIII). *Clays Clay Miner.* **18**, 203 (1970). doi:10.1346/CCMN.1970.0180404

36. M. J. McAllister *et al*., Single sheet functionalized graphene by oxidation and thermal expansion of graphite. *Chem. Mater.* **19**, 4396 (2007). doi:10.1021/cm0630800

37. R. S. Rubino, E. S. Takeuchi, The study of irreversible capacity in lithium-ion anodes prepared with thermally oxidized graphite. *J. Power Sources* **81**, 373 (1999). doi:10.1016/S0378-7753(99)00217-7

38. M. Choucair, P. Thordarson, J. A. Stride, Gram-scale production of graphene based on solvothermal synthesis and sonication. *Nat. Nanotechnol.* **4**, 30 (2009). doi:10.1038/nnano.2008.365 Medline

39. M. Kaempgen, C. K. Chan, J. Ma, Y. Cui, G. Gruner, Printable thin film supercapacitors using single-walled carbon nanotubes. *Nano Lett.* **9**, 1872 (2009). doi:10.1021/nl8038579 Medline